Photo-activation of ruthenium-decorated upconverting nanoparticles

Meijer, M.S.

CHAPTER 5

Synthesis and characterization of ruthenium trischelate complexes bearing a photocleavable bisthioether ligand

*Thioethers are good ligands for photo-activatable ruthenium(II) polypyridyl complexes, as they form thermally stable complexes that are prone to ligand substitution under visible light irradiation. Here, we introduce a novel symmetric chelating bisthioether ligand scaffold, based on 1,3-bis(methylthio)-2-propanol, **4**, and report the synthesis and stereochemical characterization of a series of novel ruthenium(II) polypyridyl complexes* $[Ru(bpy)_2(L)](PF_6)_2$, $[\mathbf{1–3}](PF_6)_2$, *where L is ligand **4**, its methyl ether, 1,3-bis(methylthio)-2-methoxypropane, **5**, or its carboxymethyl ether, 1,3-bis(methylthio)-2-(carboxymethoxy)propane, **6**. Coordination of ligands **4–6** to the bisbipyridine-ruthenium centre gives rise to 16 possible isomers, consisting of eight possible Λ diastereoisomers and their Δ enantiomers. We found that the synthesis of* $[\mathbf{1–3}](PF_6)_2$ *is diastereoselective, yielding a racemic mixture of the* Λ-(S)-eq-(S)-ax-OH_{eq}-$[\mathbf{Ru}]^{2+}$ *and* Δ-(R)-ax-(R)-eq-OH_{eq}-$[\mathbf{Ru}]^{2+}$ *isomers. Upon irradiation with blue light in water,* $[\mathbf{1–3}](PF_6)_2$ *selectively and efficiently substitute their bisthioether ligands for water molecules in a two-step photoreaction, ultimately producing cis-*$[Ru(bpy)_2(H_2O)_2]^{2+}$ *as the photoproduct. The relatively stable photochemical intermediate was identified as cis-*$[Ru(bpy)_2(\eta^1\text{-}L)(H_2O)]^{2+}$ *by mass spectrometry. The selective and efficient photochemical reaction makes the bisthioether ligand scaffold reported here a promising candidate for use as photocleavable anchoring group for the binding of ruthenium-based PACT complexes to the surface of UCNPs.*

This chapter is to be submitted as a full paper: Michael S. Meijer, Sylvestre Bonnet, *manuscript in preparation*

5.1 Introduction

The use of light as a trigger for the activation of metal-based anticancer agents has been actively researched over the last decades.[1] In combination with ruthenium(II) complexes, light can be used either to drive the formation of reactive oxygen species through the sensitization of oxygen in photodynamic therapy (PDT),[2] or to uncage photo-activatable complexes through ligand substitution in photo-activated chemotherapy (PACT).[3] This photolability can be enhanced through both steric and electronic effects.[4] In Chapters 3 and 4, we discussed the use of sterically-demanding dimethylated bidentate ligands as photocleavable ligands in ruthenium trischelate PACT complexes, designed to be excited with near-infrared light via upconverting nanoparticles (UCNPs). In those studies, we noticed that the use of strained ligands based on the rigid 1,10-phenanthroline (phen) scaffold, which are the most readily modified dinitrogen chelates for binding of the complex to the surface of UCNPs, could hamper the selectivity and efficiency of the photosubstitution reaction.

Thus, we set out to find another ligand scaffold that can be easily modified to facilitate the binding of the complex to the surface of UCNPs, but which is efficiently and selectively photosubstituted upon irradiation with visible light. In our group, studies have been undertaken towards the use of thioether ligands as photocleavable caging groups for ruthenium polypyridyl complexes.[3d,5] Their softness makes thioethers excellent ligands for ruthenium(II) ions, and their complexes often show good thermal stability. Under blue light irradiation, several groups have shown that thioether ligands can be selectively substituted by solvent molecules, both for monodentate ligands, e.g. 2-(methylthio)ethanol (Hmte),[5a,6] and for bidentate chelating thioether ligands.[3d,7] Examples of the latter include combinations of thioether sulfur donors with nitrogen donor atoms, e.g. 2-(methylthio)methylpyridine (mtmp),[3d] as well as symmetric bis(arylthioether) ligands, e.g. 1,3-bis(phenylthio)propane (bptp).[7b-d] The photosubstitution of bisthioether ligands was shown to be 5–10 times more efficient than that of comparable bis-amine ligands.[7b]

In this chapter, we report the coordination of the symmetric bidentate bisthioether ligand 1,3-bis(methylthio)-2-propanol, **4**, to ruthenium. We introduced an alcohol functionality in this ligand to allow for future functionalization; this substituent was added in a symmetrical position to prevent the formation of regioisomers upon coordination of the ligand. To exemplify these substitution options, we also

prepared the methyl- and carboxymethyl-substituted derivatives, 1,3-bis(methylthio)-2-methoxypropane, **5**, and 1,3-bis(methylthio)-2-(carboxymethoxy)propane, **6**. Ligand **6** bears a carboxylic acid group, which allows for straightforward further functionalization, for example through the formation of peptide bonds. We synthesized three new ruthenium polypyridyl complexes of the general formula $[Ru(bpy)_2(L)](PF_6)_2$ [**1–3**]$(PF_6)_2$, where bpy = 2,2'-bipyridine, and L = **4**, **5** or **6** (Scheme 5.1). We investigated the stereochemistry of the complexes using density functional theory (DFT) and NOESY NMR studies, and examined both the efficiency and selectivity of the photochemistry of complexes [**1–3**]$(PF_6)_2$ in aqueous solution. Our results are compared to reports by the groups of Turro and Sauvage on the related bisthioether chelate complexes $[Ru(bpy)_2(bete)](PF_6)_2$ ([**7**]$(PF_6)_2$, bete = 3,6-dithiaoctane), $[Ru(bpy)_2(bpte)](PF_6)_2$ ([**8**]$(PF_6)_2$, bpte = 1,2-bis(phenylthio)ethane), $[Ru(phen)_2(bpte)](PF_6)_2$ ([**9**]$(PF_6)_2$), and $[Ru(phen)_2(bptp)](PF_6)_2$ ([**10**]$(PF_6)_2$), all shown in Scheme 5.1.[7b,7c] In particular, we evaluate the effects of the chelating ring size (five- or six-membered ring), of the size and aromaticity of the thioether substituent (methyl, ethyl or phenyl group), and of the addition of a substituent to the chelating ring (i.e. the hydroxyl or ether group in complexes [**1–3**]$(PF_6)_2$) on the stereo- and photochemistry of this type of complexes.

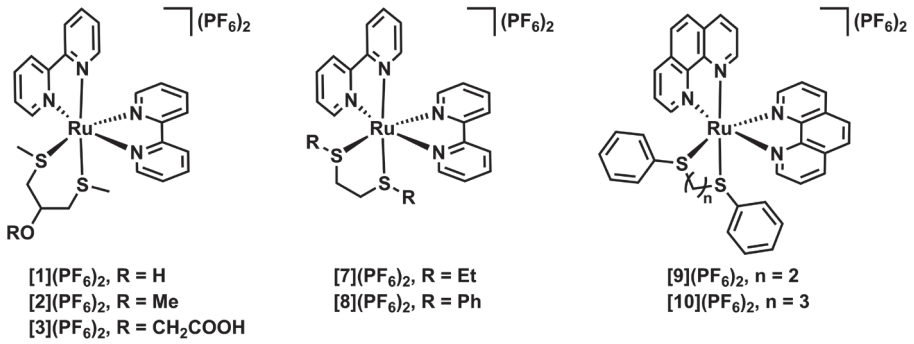

Scheme 5.1. Chemical structures of novel ruthenium polypyridyl complexes [1–3]$(PF_6)_2$ (left), and complexes [7–10]$(PF_6)_2$, previously reported by the groups of Turro (centre) and Sauvage (right).

5.2 Results and discussion

5.2.1 Synthesis

Ligands **5** and **6** were obtained in good yields from commercially available ligand **4** through deprotonation of the alcohol with sodium hydride, followed by

nucleophilic substitution using iodomethane or bromoacetic acid as the electrophile (Scheme 5.2). Coordination of the two soft, thioether donors of ligands **4–6** to the ruthenium centre was achieved by refluxing an excess of the ligand (2–10 eq.) with *cis*-[Ru(bpy)$_2$Cl$_2$] in an ethanol/water mixture. Replacement of the two coordinating chlorides by ligands **4–6** was typically completed within 1.5 h, as shown by the colour change of the solution from purple to orange. After anion exchange with KPF$_6$, complexes [**1–3**](PF$_6$)$_2$ were obtained in 55–69% yield as orange solids. The complexes were all isolated as their bishexafluoridophosphate salt, as confirmed by elemental analysis. The work-up of compound [**3**](PF$_6$)$_2$ was performed under acidic conditions (pH ≈ 2) to ensure protonation of the carboxylic acid in the final product. All three complexes were soluble in water, despite their apolar counter anions. Coordination of the bisthioether ligand was clearly observed by ^{1}H NMR by a splitting of the signal of the thiomethyl groups, e.g. from a singlet at 2.16 ppm for ligand **5** in CDCl$_3$ to two singlets at 1.63 and 1.34 ppm for complex [**2**](PF$_6$)$_2$ in acetone-*d6*. Further characterization of the complexes was performed using high-resolution mass spectrometry, elemental analysis, thin layer chromatography, and UV-Vis absorption spectroscopy (section 5.2.3).

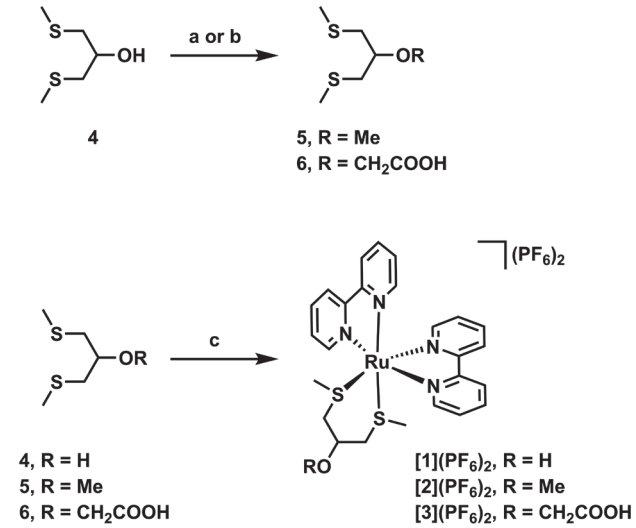

Scheme 5.2. Synthesis of ruthenium complexes [1–3](PF$_6$)$_2$. Conditions: a) NaH, iodomethane in THF, 0 °C to r.t., 24 h, 66%; b) NaH, KI, bromoacetic acid in THF, 0 °C to reflux, 22 h, 95%; c) *i. cis*-[Ru(bpy)$_2$Cl$_2$] in EtOH/H$_2$O (1:1 v/v), reflux, 1.5 h; *ii.* KPF$_6$, 57% ([1](PF$_6$)$_2$), 69% ([2](PF$_6$)$_2$), 55% ([3](PF$_6$)$_2$). Compounds [1–3](PF$_6$)$_2$ were obtained as racemic Λ/Δ-mixtures.

As we used a racemic sample of *cis*-[Ru(bpy)$_2$Cl$_2$] for the synthesis of [**1–3**](PF$_6$)$_2$, we obtained racemic mixtures of the Λ and Δ enantiomers for each complex. An additional stereochemical complication is caused by the six-membered ring formed by the coordination of ligands **4–6**, which induces four more sources of isomerism: the configuration (*R* or *S*) of the two sulfur atoms, the configuration of the carbon atom attached to the hydroxyl or ether group, leading to either an axial or equatorial –OR substituent, and the inversion of the six-membered metallacycle, which transforms all axial substituents on the ring into equatorial ones. With five stereogenic centres, we would expect thirty-two possible isomers, i.e. sixteen Λ diastereoisomers and their respective Δ enantiomers. However, due to the plane of symmetry in ligands **4–6**, inversion of the six-membered ring leads to the formation of one of the other diastereoisomers, e.g. ring inversion of Λ-a-[**Ru**]$^{2+}$ (see Scheme 5.3) leads to the formation of Λ-h-[**Ru**]$^{2+}$. Thus, we concluded that there are eight possible Λ diastereoisomers in total, shown in Scheme 5.3, all with their respective Δ enantiomers. Table 5.1 lists the enantiomeric pairs. According to 1D and 2D ^{1}H NMR, which showed only a single set of 16 aromatic proton signals originating from the bipyridine ligands, all three complexes were obtained diastereomerically pure.

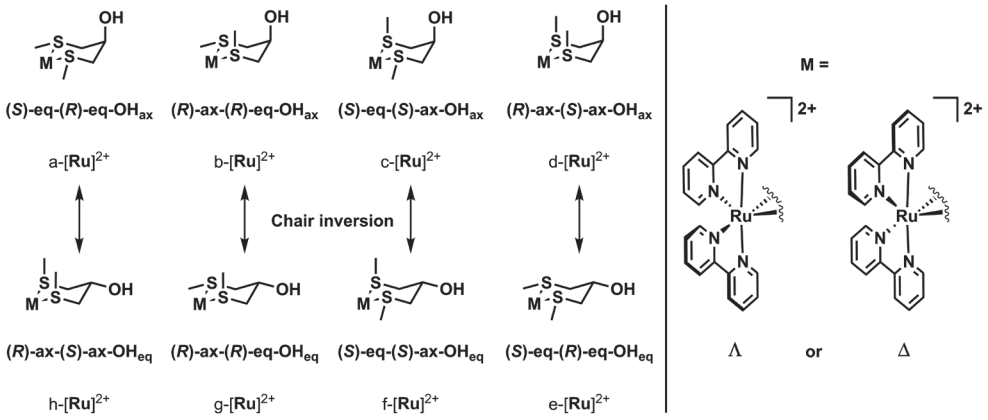

Scheme 5.3. Possible stereoisomers of complexes [1–3]$^{2+}$, resulting from the inversion of either the configuration of one of the sulfur atoms, or the configuration of the carbon atom attached to the hydroxyl or ether group.

Table 5.1. Enantiomeric pairs of the possible stereoisomers of [1–3]$^{2+}$.

Λ	Λ-a-[**Ru**]$^{2+}$	Λ-b-[**Ru**]$^{2+}$	Λ-c-[**Ru**]$^{2+}$	Λ-d-[**Ru**]$^{2+}$	Λ-e-[**Ru**]$^{2+}$	Λ-f-[**Ru**]$^{2+}$	Λ-g-[**Ru**]$^{2+}$	Λ-h-[**Ru**]$^{2+}$
Δ	Δ-a-[**Ru**]$^{2+}$	Δ-c-[**Ru**]$^{2+}$	Δ-b-[**Ru**]$^{2+}$	Δ-d-[**Ru**]$^{2+}$	Δ-e-[**Ru**]$^{2+}$	Δ-g-[**Ru**]$^{2+}$	Δ-f-[**Ru**]$^{2+}$	Δ-h-[**Ru**]$^{2+}$

5.2.2 Structural characterization by NOESY and DFT

In order to gather insight into which one of the eight diastereoisomers of [**1**](PF$_6$)$_2$ was obtained, we performed a computational study of the stability of each of these isomers in aqueous solution using DFT, employing the COSMO model to simulate solvent effects (see section 5.4.4). We minimized the structures of the eight Λ diastereoisomers of [**1**]$^{2+}$ shown in Scheme 5.3, where the six-membered ring is in a chair conformation, as well as the eight possible diastereoisomers with the six-membered ring in a boat configuration. The diastereoisomers in boat configuration either relaxed to one of the chair configurations shown above, or resulted in a twisted-boat configuration with a high energy. Thus, we concluded that a boat configuration is energetically strongly disfavoured for the six-membered metallacycle in [**1**]$^{2+}$, and that the product obtained must be in a chair configuration. The optimized structures, their structural distortion parameters, and their respective energies in water are given in Table 5.2, Table SV.1, and Figure SV.6. Four of the possible geometries, i.e. Λ-b-[**1**]$^{2+}$, Λ-d-[**1**]$^{2+}$, Λ-g-[**1**]$^{2+}$, and Λ-h-[**1**]$^{2+}$, were significantly higher in energy, compared to the other four. All of these geometries have one of the sulfur atoms in a (*R*)-ax orientation that leads to a steric clash of the thiomethyl group with one of the bipyridine ligands (Figure SV.6). Diastereoisomer Λ-(*S*)-eq-(*S*)-ax-OH$_{eq}$-[**1**]$^{2+}$ (Λ-f-[**1**]$^{2+}$ in Scheme 5.3) is the lowest in energy, 3.7 kJ·mol^{-1} lower in energy than the diastereoisomer that is second lowest in energy, Λ-(*S*)-eq-(*S*)-ax-OH$_{ax}$-[**1**]$^{2+}$ (Λ-c-[**1**]$^{2+}$), obtained by inversion of the configuration of the carbon atom bearing the alcohol substituent. Two more diastereoisomers have relatively low energies, namely Λ-(*S*)-eq-(*R*)-eq-OH$_{ax}$-[**1**]$^{2+}$ (Λ-a-[**1**]$^{2+}$), and Λ-(*S*)-eq-(*R*)-eq-OH$_{eq}$-[**1**]$^{2+}$ (Λ-e-[**1**]$^{2+}$), where both thiomethyl groups are found in equatorial positions. The small energy differences of ~4 kJ·mol^{-1} between these isomers is not enough to exclude any of these four structures purely based on their computed energies.

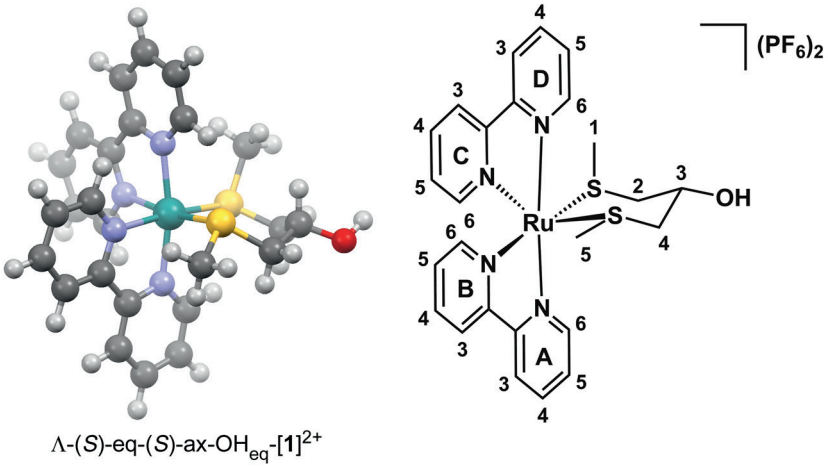

Figure 5.1. Structure of the most stable Λ diastereoisomer of $[1]^{2+}$, Λ-(*S*)-eq-(*S*)-ax-OH_{eq}-$[1]^{2+}$ (Λ-f-$[1]^{2+}$), optimized by DFT (BLYP/TZP) in water (COSMO), with a schematic drawing showing the atom numbering used in the text.

Table 5.2. Absolute and relative energies in water (COSMO) of the Λ diastereoisomers of $[1]^{2+}$, optimized by DFT.

Isomer	Absolute energy in water / Hartree	Relative energy (*ΔE*) in water / kJ·mol^{-1}
Λ-a-$[\mathbf{1}]^{2+}$	-13.05674	4.1
Λ-b-$[\mathbf{1}]^{2+}$	-13.05197	16.7
Λ-c-$[\mathbf{1}]^{2+}$	-13.05690	3.7
Λ-d-$[\mathbf{1}]^{2+}$	-13.05133	18.4
Λ-e-$[\mathbf{1}]^{2+}$	-13.05688	3.8
Λ-f-$[\mathbf{1}]^{2+}$	-13.05832	0.0
Λ-g-$[\mathbf{1}]^{2+}$	-13.05310	13.7
Λ-h-$[\mathbf{1}]^{2+}$	-13.05317	13.5

As the DFT calculations did not provide a conclusive answer, we turned to ^{1}H NMR spectroscopy. The stereochemistry of the carbon atom bearing the alcohol (C_3 in Figure 5.1) could be found from the ^{3}J coupling constants of the protons on the adjacent carbon atom (C_2). The large difference between the ^{3}J coupling constant of the axial (^{3}J = 6.3 Hz) and equatorial protons (^{3}J = 2.1 Hz), suggests that the proton on C_3 is positioned axially, and thus the –OH group has to be equatorial. NOESY NMR spectroscopy further confirmed the axial position of this proton (H_3) by an off-diagonal correlation with the D6 proton of the bpy ligand (Figure SV.1). As the alcohol group is equatorial, the number of possible Λ-isomers of $[\mathbf{1}]^{2+}$ in solution was reduced to two, i.e. Λ-(*S*)-eq-(*S*)-ax-OH_{eq}-$[\mathbf{1}]^{2+}$ (Λ-f-$[\mathbf{1}]^{2+}$) and

Λ-(*S*)-eq-(*R*)-eq-OH$_{eq}$-[**1**]$^{2+}$ (Λ-e-[**1**]$^{2+}$), which differ from each other by a single inversion of sulfur chirality. In order to assess whether this thiomethyl group (C_1 in Figure 5.1) was axial or equatorial, we examined the off-diagonal NOESY correlations of this group (Figure SV.2). We found a correlation of these protons to the A6 proton of the bpy ligand, over a distance of 3.29 Å *versus* 5.00 Å for the equatorial and axial cases, respectively. This suggested that the thiomethyl group is oriented equatorially. However, the protons on C_1 also show an off-diagonal correlation to the axial proton on C_3, a proton that is significantly closer if the thiomethyl group is oriented axially (3.36 Å *versus* 4.98 Å). Finally, a weak correlation to the C3 proton on the bipyridine ring, which is closer to thiomethyl group C_1 in the axial conformation (5.19 Å *versus* 6.22 Å), convinced us that this thiomethyl group is most likely oriented axially. All in all, our NMR studies suggest that [**1**]$^{2+}$ is a racemic mixture of Λ-(*S*)-eq-(*S*)-ax-OH$_{eq}$-[**1**]$^{2+}$ (Λ-f-[**1**]$^{2+}$, Figure 5.1) and Δ-(*R*)-ax-(*R*)-eq-OH$_{eq}$-[**1**]$^{2+}$ (Δ-g-[**1**]$^{2+}$). This is also the enantiomeric pair that was found to be most stable in our DFT studies (Table 5.2), suggesting that the formation of the complex is under thermodynamic control. NMR studies of complexes [**2**]$^{2+}$ and [**3**]$^{2+}$ in solution showed that substitution of the alcohol does not affect the stereochemistry of the complexes, as these complexes were also found to be a racemic mixture of Λ-f-[**Ru**]$^{2+}$ and Δ-g-[**Ru**]$^{2+}$ enantiomers, where [**Ru**]$^{2+}$ is [**2**]$^{2+}$ or [**3**]$^{2+}$.

In recent work from our group we have shown that the bond angle variance σ^2, can be used as a structural distortion parameter to quantify the steric hindrance induced by thiomethyl groups in ruthenium polypyridyl complexes that bear no straining pyridyl ligands.[7a,8] In the case of complex [**1**]$^{2+}$, we observed an increase of the σ^2 value by at least 25 upon the introduction of an (*R*)-ax sulfur atom in the Λ diastereoisomers, compared to their corresponding (*S*)-eq isomer (e.g. σ^2 = 59.4 and 87.5 for Λ-a-[**1**]$^{2+}$ and Λ-b-[**1**]$^{2+}$, respectively, see Table SV.1). This correlates well with the energies calculated by DFT (Table 5.2), which show an increase by 10–15 kJ·mol^{-1} for this inversion of the sulfur configuration. Interestingly, we could not find a direct correlation between the σ^2 value and the DFT energy for the conformation of the second sulfur atom. Inversion from Λ-(*S*)-ax to Λ-(*R*)-eq for the C_1 thiomethyl group led to an increase in the σ^2 value of ~17, but resulted in virtually no increase in DFT-calculated energy. This phenomenon could be explained by the fact that the calculation of the σ^2 value does not take into account the intraligand interactions within ligand **4**. Although the Λ-(*S*)-ax conformation is favourable for relieving the octahedral strain on the ruthenium centre, it does lead

to unfavourable 1,3-diaxial interactions with the H_3 proton on ligand **4**, making the total energetic effect negligible. Logically, we observed no effect of orientation of the alcohol group on the σ^2 value, since this does not affect the octahedral strain on the ruthenium centre.

The synthesis of the related complexes [**9**]$(PF_6)_2$ and [**10**]$(PF_6)_2$ was also reported to be diastereoselective by Sauvage *et al.*, who reported the same stereochemistry for the sulfur atoms as we found for [**1–3**]$(PF_6)_2$.[7c] However, in their crystal structure the six-membered ring in [**10**]$(PF_6)_2$ is found in a half-chair conformation, perhaps made possible by the lack of substitution at the C_3 position. Overall, we can conclude that the configuration of the sulfur atoms is not influenced by the size of the ring, nor by the type of substituents on the sulfur atoms (methyl groups in [**1–3**]$(PF_6)_2$ and phenyl groups in [**9–10**]$(PF_6)_2$) or by substituents on the chelating ring. However, the introduction of the substituents to the C_3 position on the ring does seem to force the ring into a chair conformation.

5.2.3 Photochemistry

All three complexes form yellow solutions in water, showing a ^{1}MLCT absorption band around 412 nm, with molar absorption coefficients of 4.0–5.2 × 10^3 $M^{-1}\cdot cm^{-1}$ (Table 5.3), typical for ruthenium(II) polypyridyl complexes containing two thioether donor ligands.[7b] Essentially no phosphorescence was observed upon irradiation of the complexes with blue light in deuterated methanol (Figure SV.7a), with phosphorescence quantum yields Φ_P lower than 2.0 × 10^{-4}. The complexes also appeared to be very poor singlet oxygen sensitizers ($\Phi_\Delta \leq 0.008$, Figure SV.7b), as expected from their photosubstitution properties (*vide infra*).

Table 5.3. Lowest-energy absorption maxima (λ_{max}), molar absorption coefficients at λ_{max} (ε_{max}) and 443 nm (ε_{443}), photosubstitution quantum yields (Φ_{443}) and photosubstitution reactivities ($\xi_{443} = \Phi_{443} \times \varepsilon_{443}$) at 298 K in H_2O, singlet oxygen quantum yield (Φ_Δ) and phosphorescence quantum yield (Φ_P) at 293 K in MeOD for complexes [1–3]$(PF_6)_2$ and photochemical intermediates [11–13]$(PF_6)_2$.

Complex	λ_{max} / nm (ε_{max} / $M^{-1}\cdot cm^{-1}$)	ε_{443} / $M^{-1}\cdot cm^{-1}$	Φ_{443}	ξ_{443}	Φ_Δ	Φ_P (λ_{em} / nm)
[1]$(PF_6)_2$	413 (5.13 × 10^3)	2.95 × 10^3	0.24	704	0.008	2.0 × 10^{-4} (624)
[11]$(PF_6)_2$	453 (7.02 × 10^3)	6.68 × 10^3	0.0079	53	-	-
[2]$(PF_6)_2$	412 (4.04 × 10^3)	2.29 × 10^3	0.25	578	0.007	1.4 × 10^{-4} (620)
[12]$(PF_6)_2$	456 (5.52 × 10^3)	5.04 × 10^3	0.0093	47	-	-
[3]$(PF_6)_2$	412 (5.18 × 10^3)	2.92 × 10^3	0.16	474	< 0.005	6 × 10^{-5} (620)
[13]$(PF_6)_2$	456 (6.77 × 10^3)	6.19 × 10^3	0.0055	34	-	-

In the absence of light, complexes [**1–3**]$(PF_6)_2$ were found to be stable in water (Figure SV.5). However, all three compounds are photoreactive under blue light irradiation in water. We monitored the photoreactions of [**1–3**]$(PF_6)_2$ with UV-Vis absorption spectroscopy and mass spectrometry. Upon irradiation of a solution of [**1**]$(PF_6)_2$ with a blue LED (λ = 443 ± 11 nm) we observed a two-step bathochromic shift in the ^{1}MLCT absorbance band of the solution (Figure 5.2). Firstly, the absorption maximum shifted from 413 to 453 nm, accompanied by three isosbestic points at 319, 364 and 426 nm. This first reaction was completed within 5 minutes under the irradiation conditions used (photon flux $q_p = 2.65 \times 10^{-8}$ mol photons·s^{-1}), at which point the absorption maximum started to shift towards longer wavelengths again. This second reaction, in which the absorption maximum changed from 453 to 491 nm, showed isosbestic points at 314, 330, 389, and 466 nm, and was significantly slower than the first photoreaction. Completion of this second reaction took an hour, at which point a steady state was reached. Mass spectrometry of the reaction mixture after irradiation (Figure SV.9) showed a peak at m/z = 247.9, corresponding to $[Ru(bpy)_2(CH_3CN)_2]^{2+}$ (calcd. m/z = 248.0), formed inside the mass spectrometer from the original photoproduct $[Ru(bpy)_2(OH_2)_2]^{2+}$ ([**14**]$^{2+}$). No signals were observed that match to photoproducts resulting from expulsion of one of the bpy ligands. This result indicates that upon blue-light irradiation of [**1**]$^{2+}$ in water, the bisthioether chelate **4** is selectively substituted by two water molecules.

The intermediate species in the photoreaction was identified by mass spectrometry, by measuring a sample after the first five minutes of irradiation (Figure SV.8). This sample showed the peak for the photoproduct, as well as a peak for the starting compound [**1**]$^{2+}$ at m/z = 282.7 (calcd. m/z = 283.0), and another signal at m/z = 303.1, identified as $[Ru(bpy)_2(\mathbf{4})(CH_3CN)]^{2+}$ (calcd. m/z = 303.6), formed inside the mass spectrometer from the original photochemical intermediate $[Ru(bpy)_2(\mathbf{4})(H_2O)]^{2+}$. We hypothesized that the intermediate, which is reasonably stable, is most likely six-coordinate, with ligand **4** bound in a monodentate fashion, and the second thioether group replaced by water, i.e. $[Ru(bpy)_2(\eta^1\text{-}\mathbf{4})(H_2O)]^{2+}$ ([**11**]$^{2+}$). On a whole, under blue light irradiation [**1**]$(PF_6)_2$ undergoes a two-step consecutive photochemical substitution of the bis-thioether ligand, passing through the rather stable mono-aqua intermediate [**11**]$^{2+}$ (Scheme 5.4). This two-step photoreactivity is reminiscent of the photoreactivity observed for ruthenium polypyridyl complexes bearing two photocleavable monodentate ligands, such as *cis*-$[Ru(bpy)_2(py)_2]^{2+}$ (py = pyridine),[9] and has also been observed for the

photodissociation of the ligand bete in $[\mathbf{7}]^{2+}$,[7b] or mtmp (2-(methylthio)methyl-2-pyridine) in $[Ru(bpy)_2(mtmp)]^{2+}$.[3d]

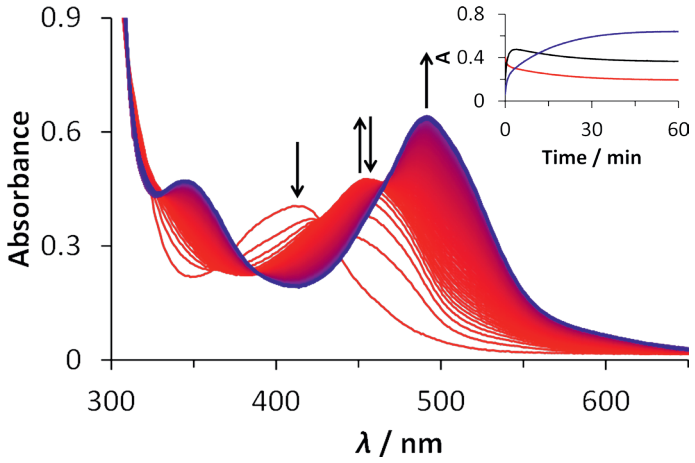

Figure 5.2. Evolution of the UV-Vis absorption spectra of a solution of $[\mathbf{1}](PF_6)_2$ in H_2O (72 μM) upon irradiation (120 min) at 298 K with a 443 nm LED (q_P = 2.65 × 10^{-8} mol photons·s^{-1}) under N_2. Inset: Time evolution of the absorbance at 413 nm (red), 453 nm (black) and 491 nm (blue) during the first 60 min of irradiation.

Irradiation of complexes $[\mathbf{2}]^{2+}$ and $[\mathbf{3}]^{2+}$ resulted in very similar photoreactions, as shown in Figure SV.3 and Figure SV.4. The UV-Vis absorption spectra indicate formation of the same final photoproduct $[\mathbf{14}]^{2+}$, passing through the monodentate photochemical intermediates $[\mathbf{12}]^{2+}$ and $[\mathbf{13}]^{2+}$. The quantum efficiencies of the two photochemical steps for each photoreaction was derived using global fitting of the time evolution of the UV-Vis absorption spectra, using the Glotaran software package (Table 5.3, Figure SV.10, Figure SV.11, and Figure SV.12).[10] The photosubstitution quantum yields Φ_{443} were found to be similar across all three complexes, with Φ_{443} = 0.24, 0.25 and 0.16 for the first step of the photoreaction for $[\mathbf{1}]^{2+}$, $[\mathbf{2}]^{2+}$ and $[\mathbf{3}]^{2+}$, respectively. The second step of the photoreaction was characterized by photosubstitution quantum yields of 0.0079, 0.0093 and 0.0055, respectively. These quantum efficiencies are similar to those observed earlier for the second reaction step of bidentate pyridine-thioether ligands,[3d] and slightly lower than those found for the substitution of monodentate thioether ligands.[5a] For the photosubstitution reactions of $[\mathbf{7}]^{2+}$ and $[\mathbf{8}]^{2+}$ in water, Turro *et al.* also reported a two-step mechanism, including a quick formation of a η^1-coordinated intermediate species. They reported overall quantum yields for the formation of $[\mathbf{14}]^{2+}$ (Φ_{400}), of 0.024 and 0.022, respectively, rather than the quantum yields of the

individual steps reported above for the photosubstitution reactions in [**1–3**]$^{2+}$.[7b] Unfortunately, this precludes a direct comparison of the efficiencies.

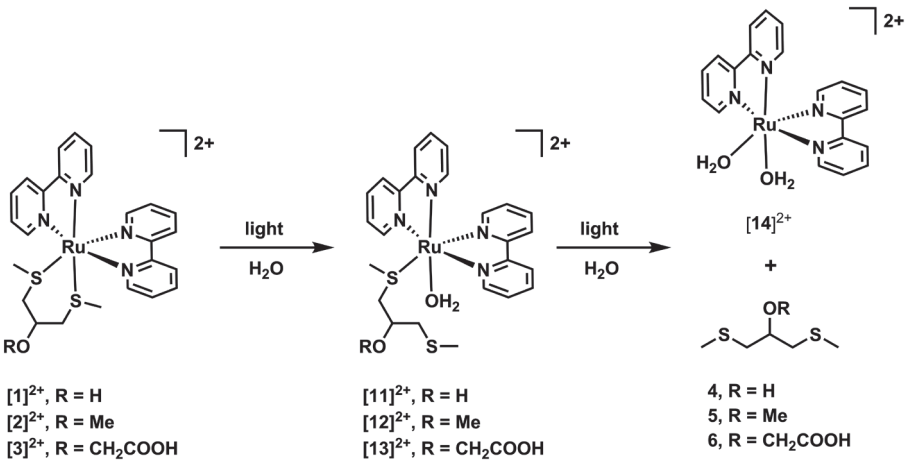

Scheme 5.4. Two-step photosubstitution reactions observed upon blue light irradiation of solutions of [1]$^{2+}$, [2]$^{2+}$, and [3]$^{2+}$ in H_2O.

5.3 Conclusion

In this work, we have shown that the coordination of ligands **4**, **5** and **6** to the *cis*-Ru(bpy)$_2$ scaffold under reflux in an EtOH/H_2O mixture is diastereoselective, yielding complexes [**1–3**]$(PF_6)_2$ as a racemic mixture of two enantiomers, namely Λ-(*S*)-eq-(*S*)-ax-OH$_{eq}$-[**Ru**]$^{2+}$ and Δ-(*R*)-ax-(*R*)-eq-OH$_{eq}$-[**Ru**]$^{2+}$. DFT calculations showed this isomer to be the most energetically favourable, suggesting that the synthesis is under thermodynamic control in such conditions. As the obtained isomer was also found to have the smallest bond angle variance (σ^2), we hypothesize that minimization of the steric hindrance induced by the thioether ligands is a major driving force for the formation of this isomer. However, as we obtained the same diastereoisomer that was reported for complexes [**9**]$(PF_6)_2$ and [**10**]$(PF_6)_2$, we conclude that the diastereoselectivity is not determined by the nature of the thioether substituent, nor by the chelate ring size. According to DFT, the substituent on the C_3 carbon in [**1–3**]$(PF_6)_2$ does force the chelate ring in a chair conformation, rather than a half-chair conformation as observed in the X-ray structures of [**9**]$(PF_6)_2$ and [**10**]$(PF_6)_2$.

All three complexes were found to be stable in the dark in aqueous solution, but undergo efficient ligand substitution reactions upon irradiation with blue light. In all three cases, a selective substitution of the bisthioether ligand in two steps was

observed, leading to the formation of the bis-aquated complex $[Ru(bpy)_2(H_2O)_2]^{2+}$ ($[\mathbf{14}]^{2+}$). The reaction mechanism was found to be identical to that reported for complexes $[\mathbf{7}](PF_6)_2$ and $[\mathbf{8}](PF_6)_2$. A thirty-fold difference in efficiency between the two steps of the photoreaction was observed, which, combined with a high time-resolution in the irradiation experiments, allowed us to determine the photosubstitution quantum yields for the individual steps, rather than the overall quantum yield. It also allowed us to identify the photochemical intermediate as the mono-thioether, mono-aqua complex by mass spectrometry.

Substitution of the alcohol, as in complexes $[\mathbf{2}](PF_6)_2$ and $[\mathbf{3}](PF_6)_2$, does not have an effect on the diastereoselectivity of the synthesis, nor on the selectivity of the photosubstitution reaction. Only small differences were observed in the efficiency of the photosubstitution reactions. Thus, functionalized bisthioether ligands are promising candidates for use as photocleavable ligands for the binding of ruthenium-based PACT complexes to inorganic surfaces, such as that of UCNPs, which will be further discussed in Chapter 6.

5.4 Experimental

5.4.1 General

Dry tetrahydrofuran (THF) was collected from a Pure Solve MD5 dry solvent dispenser (Demaco). 1,3-bis(methylthio)-2-propanol (**4**) was obtained from Alfa Aesar. All other reagents and solvents, including *cis*-$[Ru(bpy)_2Cl_2]$, were purchased from Sigma-Aldrich, and used as received. All synthesis was conducted in oxygen-free atmosphere using standard Schlenk line techniques. Synthesis of all ruthenium complexes was performed in the absence of light. Flash column chromatography was performed on silica gel (Screening devices B.V.) with a particle size of 40–64 μm and a pore size of 60 Å. TLC analysis was conducted on TLC aluminium foils with silica gel matrix (Supelco, silica gel 60, art. nr. 56524) with detection by UV-absorption (254 nm) or basic $KMnO_4$ spray. Size exclusion column chromatography was performed in acetone using Sephadex LH20, loaded into a chromatography column ($\varnothing$ = 3–4 cm, $l \approx 60$ cm).

All NMR spectra were recorded on a Bruker AV-300, AV-400 or AV-500 spectrometer. Chemical shifts (δ) are indicated in ppm relative to TMS or the solvent peak. Mass spectra were recorded by using a MSQ Plus Spectrometer fitted with a Dionex automatic sample injection system. High resolution mass spectra were recorded by direct injection (2 μl of 1 μM solution in MeOH or acetonitrile and 0.1% formic acid) in a mass spectrometer (Thermo Finnigan LTQ Orbitrap) equipped with an electrospray (250 °C) with resolution R = 60,000 at m/z = 400 (mass range m/z = 150–2000) and dioctylphthalate (m/z = 391.28428) as a lock mass. The high-resolution mass spectrometer was calibrated prior to measurements with a calibration mixture (Thermo Finnigan).

5.4.2 Ligand synthesis

1,3-bis(methylthio)-2-methoxypropane, 5: Dry and deoxygenated THF (20 mL) was added under dinitrogen atmosphere to a round-bottom flask containing 1,3-bis(methylthio)-2-propanol (0.56 g,

0.50 mL, 3.70 mmol), followed by the addition of solid NaH (296 mg, 7.40 mmol, 60% dispersion in mineral oil). The resulting suspension was stirred at RT for 20 min to allow complete deprotonation of the alcohol. Afterwards the reaction mixture was cooled to 0 °C, and iodomethane (0.63 g, 0.28 mL, 4.44 mmol) was added dropwise. The resulting suspension was stirred at RT for 24 h, and then quenched with sat. aq. NH_4Cl (5 mL) to yield a light yellow solution. The solvent was removed *in vacuo*, and the residue was dissolved in H_2O (40 mL), and extracted to DCM (3 × 40 mL). The organic layers were combined, washed with brine, dried over $MgSO_4$, and concentrated by rotary evaporation. Separation of the product (R_f = 0.7) and unreacted starting compound (R_f = 0.9) was performed by column chromatography (SiO_2, petroleum ether 40/60:EtOAc (4:1)), ultimately resulting in 404 mg of compound **5** as a colourless oil (2.43 mmol, 66%). ^{1}H NMR (400 MHz, δ in $CDCl_3$): 3.50 (p, J = 5.7 Hz, 1H, H_3), 3.42 (s, 3H, H_6), 2.74 (ddd, J = 21.4, 13.6, 5.7 Hz, 4H, H_2+H_4), 2.16 (s, 6H, H_1+H_5); ^{13}C NMR (101 MHz, δ in $CDCl_3$): 80.6 (C_3), 57.5 (C_6), 37.2 (C_2+C_4), 16.8 (C_1+C_5); ESI-MS in CH_3OH m/z exp. (calc.): 205.0 (205.0, $[M+K]^+$). ^{1}H NMR matches to literature data.[11]

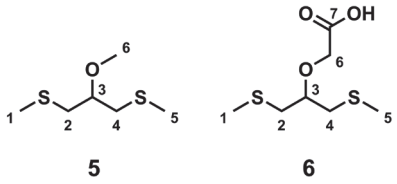

5 **6**

Scheme 5.5. Structural formulas of compounds 5, and 6, showing the atom numbering used in NMR attribution.

1,3-bis(methylthio)-2-(carboxymethoxy)propane, 6: Dry and deoxygenated THF (10 mL) was added under nitrogen atmosphere to a round-bottom flask containing 1,3-bis(methylthio)-2-propanol (0.25 g, 0.22 mL, 1.64 mmol), followed by the addition of solid NaH (328 mg, 8.20 mmol, 60% dispersion in mineral oil) and potassium iodide (22 mg, 0.133 mmol). The resulting suspension was stirred at RT for 20 min to allow complete deprotonation of the alcohol. Afterwards the reaction mixture was cooled to 0 °C, and a solution of bromoacetic acid (342 mg, 2.46 mmol) in dry THF (2 mL) was added dropwise. The resulting suspension was heated to reflux and stirred for 22 h, and subsequently cooled to 0 °C and quenched with water (10 mL) to yield a light yellow solution. The solvent was removed *in vacuo*, and the residue was dissolved in H_2O (30 mL) and washed with EtOAc (3 × 30 mL). The aqueous layer was acidified to pH ≈ 2 with 1M HCl, followed by extraction with EtOAc (3 × 50 mL). The organic layers were combined, washed with brine, dried over $MgSO_4$, and concentrated by rotary evaporation. Acetic acid impurities were removed from the crude product by co-evaporation with toluene (3 × 50 mL), to obtain compound **6** as a colourless oil (327 mg, 1.55 mmol, 95%). ^{1}H NMR (300 MHz, δ in $CDCl_3$): 9.23 (s, 1H, –COOH), 4.28 (s, 2H, H_6), 3.64 (p, J = 5.9 Hz, 1H, H_3), 2.76 (ddd, J = 19.3, 14.2, 5.5 Hz, 4H, H_2+H_4), 2.15 (s, 6H, H_1+H_5); ^{13}C NMR (75 MHz, δ in $CDCl_3$): 173.4 (C_7), 79.8 (C_3), 67.5 (C_6), 37.9 (C_2+C_4), 16.6 (C_1+C_5); HR-MS in CH_3OH m/z exp. (calc.): 233.0285 (233.0384, $[M+Na]^+$).

5.4.3 Ruthenium complex synthesis

$[Ru(bpy)_2(4)](PF_6)_2$, [1]$(PF_6)_2$: A mixture of 1,3-bis(methylthio)-2-propanol (**4**, 78 mg, 0.51 mmol) and *cis*-$Ru(bpy)_2Cl_2$ (50 mg, 0.103 mmol) was placed in a 25-mL round-bottom flask, and placed under N_2 atmosphere. A deoxygenated mixture of EtOH and H_2O (1:1 v/v, 10 mL) was added, and the reaction mixture was refluxed in the dark for 1.5 h. The resulting orange solution was cooled to RT, and EtOH was removed *in vacuo*. Water (10 mL) was added to the residue, before washing with Et_2O (3 × 15 mL). Saturated aq. KPF_6 solution (~ 5 mL) was then added to the aqueous layer, and the resulting orange

suspension was extracted to DCM (6 × 20 mL). The combined organic layers were washed once with half sat. aq. KPF_6, and then dried by rotary evaporation. Any excess KPF_6 was removed by size exclusion chromatography in acetone, and after drying overnight in high vacuum, complex [**1**]$(PF_6)_2$ was obtained as an orange powder (50 mg, 0.058 mmol, 57%). TLC: R_f = 0.2 (SiO_2, acetone:H_2O:sat. aq. KPF_6 (16:4:1)); ^{1}H NMR (500 MHz, δ in acetone-*d6*): 9.87 (d, J = 5.1 Hz, 1H, H_{A6}), 9.63 (d, J = 5.6 Hz, 1H, H_{D6}), 8.88 (t, J = 8.1 Hz, 2H, H_{D3}+H_{A3}), 8.74 (dd, J = 8.2, 3.5 Hz, 2H, H_{B3}+H_{C3}), 8.47 (tdd, J = 7.9, 2.9, 1.4 Hz, 2H, H_{D4}+H_{A4}), 8.18 (td, J = 7.9, 1.5 Hz, 2H, H_{B4}+H_{C4}), 8.08 (dddd, J = 11.2, 7.4, 5.7, 1.4 Hz, 2H, H_{D5}+H_{A5}), 7.84 (d, J = 5.8 Hz, 1H, H_{B6}), 7.79 (d, J = 5.3 Hz, 1H, H_{C6}), 7.52 (tdd, J = 7.2, 5.6, 1.3 Hz, 2H, H_{B5}+H_{C5}), 5.33 (d, J = 4.4 Hz, 1H, –OH), 4.87 (br s, 1H, H_3), 3.41 (dd, J = 13.5, 3.1 Hz, 1H, $H_{4,eq}$), 3.30 (dd, J = 13.1, 6.3 Hz, 1H, $H_{2,ax}$), 3.01 (dd, J = 13.1, 2.1 Hz, 1H, $H_{2,eq}$), 2.99 – 2.93 (m, 1H, $H_{4,ax}$), 1.59 (s, 3H, H_5), 1.36 (s, 3H, H_1); ^{13}C NMR (101 MHz, δ in acetone-*d6*): 158.8, 158.7, 157.6, 157.5 (all C_q), 154.6 (C_{D6}), 154.4 (C_{A6}), 152.2 (C_{C6}), 152.1 (C_{B6}), 140.0 (C_{A4}+C_{B4}+C_{C4}+C_{D4}), 129.7, 129.1 (C_{A5}+C_{D5}), 128.9, 128.8 (C_{B5}+C_{C5}), 126.0, 125.9 (C_{A3}+C_{D3}), 125.3, 125.2 (C_{B3}+C_{C3}), 67.0 (C_3), 41.2 (C_2), 39.5 (C_4), 18.0 (C_5), 16.1 (C_1); HR-MS in CH_3CN m/z exp. (calc.): 303.5503 (303.5504, $[M-2PF_6+CH_3CN]^{2+}$), 565.0662 (565.0669, $[M-2PF_6-H]^+$); UV-Vis: λ_{max} (ε in $M^{-1}\cdot cm^{-1}$) in H_2O: 413 nm (5.13×10^3); Elemental analysis for $C_{25}H_{28}F_{12}N_4OP_2RuS_2\cdot H_2O$: (calc.): C, 34.37; H, 3.46; N, 6.41; (exp.): C, 34.94; H, 3.61; N, 6.36.

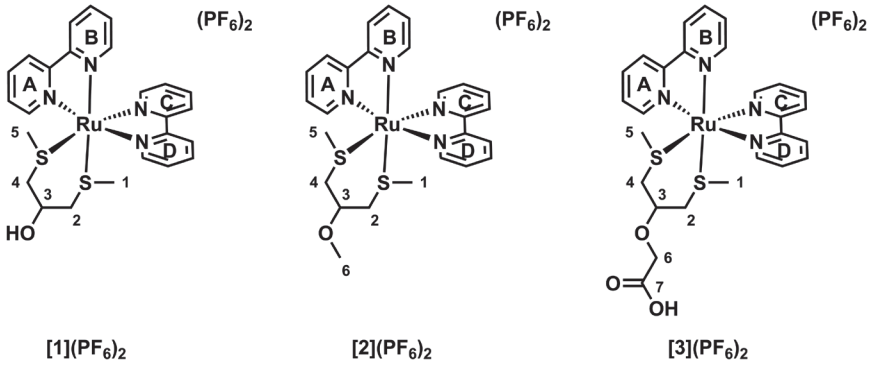

Scheme 5.6. Structural formulas of compounds [1]$(PF_6)_2$, [2]$(PF_6)_2$, and [3]$(PF_6)_2$, showing the atom numbering used in NMR attribution.

[Ru(bpy)$_2$(5)](PF$_6$)$_2$, [2](PF$_6$)$_2$: Complex [**2**]$(PF_6)_2$ was synthesized using the method described for [**1**]$(PF_6)_2$, using a mixture of **5** (85 mg, 0.516 mmol) and *cis*-Ru(bpy)$_2$Cl$_2$ (25 mg, 0.052 mmol) in a mixture of EtOH and H_2O (1:1 v/v, 6 mL). The complex was obtained as a light orange powder in 69% yield (31 mg, 0.036 mmol). TLC: R_f = 0.2 (SiO_2, acetone:H_2O:sat. aq. KPF_6 (16:4:1)); ^{1}H NMR (300 MHz, δ in acetone-*d6*): 9.81 (d, J = 5.1 Hz, 1H, H_{A6}), 9.58 (d, J = 5.3 Hz, 1H, H_{D6}), 8.88 (t, J = 7.5 Hz, 2H, H_{D3}+H_{A3}), 8.74 (dd, J = 8.2, 4.0 Hz, 2H, H_{B3}+H_{C3}), 8.46 (t, J = 7.9 Hz, 2H, H_{D4}+H_{A4}), 8.23 – 8.04 (m, 4H, H_{B4}+H_{C4}+H_{D5}+H_{A5}), 7.84 (d, J = 6.2 Hz, 1H, H_{B6}), 7.79 (d, J = 5.8 Hz, 1H, H_{C6}), 7.51 (tdd, J = 7.4, 5.6, 1.3 Hz, 2H, H_{B5}+H_{C5}), 4.48 (br s, 1H, H_3), 3.54 (s, 3H, H_6), 3.53 – 3.44 (m, 2H, $H_{4,eq}$+$H_{2,ax}$), 3.16 (dd, J = 13.7, 5.6 Hz, 1H, $H_{4,ax}$), 2.97 (dd, J = 13.2, 1.6 Hz, 1H, $H_{2,eq}$), 1.63 (s, 3H, H_5), 1.34 (s, 3H, H_1); ^{13}C NMR (75 MHz, δ in acetone-*d6*): 158.8, 158.6, 157.6, 157.5 (all C_q), 155.0 (C_{D6}), 154.1 (C_{A6}), 152.3 (C_{C6}), 152.1 (C_{B6}), 140.0, 140.0, 140.0, 140.0 (C_{A4}+C_{B4}+C_{C4}+C_{D4}), 129.8, 129.0 (C_{A5}+C_{D5}), 128.9, 128.8 (C_{B5}+C_{C5}), 126.0, 125.9 (C_{A3}+C_{D3}), 125.3, 125.2 (C_{B3}+C_{C3}), 75.8 (C_3), 57.2 (C_6), 37.6 (C_2), 36.9 (C_4), 18.2 (C_5), 15.8 (C_1); HR-MS in CH_3CN m/z exp. (calc.): 310.5584 (310.5583, $[M-2PF_6+CH_3CN]^{2+}$); UV-Vis: λ_{max} (ε in $M^{-1}\cdot cm^{-1}$) in H_2O: 412 nm (4.04×10^3); Elemental analysis for $C_{26}H_{30}F_{12}N_4OP_2RuS_2\cdot 5H_2O$: (calc.): C, 32.54; H 4.20; N, 5.84; (exp.): C, 34.00; H, 4.47; N, 5.98.

[Ru(bpy)$_2$(6)](PF$_6$)$_2$, [3](PF$_6$)$_2$: Complex [**3**](PF$_6$)$_2$ was synthesized using the method described for [**1**](PF$_6$)$_2$, using a mixture of **6** (48 mg, 0.228 mmol) and *cis*-Ru(bpy)$_2$Cl$_2$ (52 mg, 0.107 mmol) in a mixture of EtOH and H$_2$O (1:1 v/v, 10 mL). The complex was obtained as a light orange powder in 55% yield (54 mg, 0.059 mmol). TLC: R_f = 0.2 (SiO$_2$, acetone:H$_2$O:sat. aq. KPF$_6$ (16:4:1)); ^{1}H NMR (400 MHz, δ in acetone-*d6*): 9.91 (d, J = 5.6 Hz, 1H, H$_{A6}$), 9.55 (d, J = 5.2 Hz, 1H, H$_{D6}$), 8.86 (dd, J = 14.6, 8.2 Hz, 2H, H$_{D3}$+H$_{A3}$), 8.73 (t, J = 7.8 Hz, 2H, H$_{B3}$+H$_{C3}$), 8.46 (qd, J = 8.0, 1.5 Hz, 2H, H$_{D4}$+H$_{A4}$), 8.17 (tt, J = 7.9, 1.5 Hz, 2H, H$_{B4}$+H$_{C4}$), 8.06 (ddd, J = 7.4, 5.7, 1.4 Hz, 2H, H$_{D5}$+H$_{A5}$), 7.84 (dd, J = 5.7, 0.8 Hz, 1H, H$_{B6}$), 7.78 (dd, J = 5.7, 0.8 Hz, 1H, H$_{C6}$), 7.52 (dddd, J = 8.8, 7.2, 5.6, 1.3 Hz, 2H, H$_{B5}$+H$_{C5}$), 4.77 (s, 1H, H$_3$), 4.48 (d, J = 16.5 Hz, 1H, H$_6$), 4.35 (d, J = 16.5 Hz, 1H, H$_6$), 3.59 (dd, J = 13.2, 6.3 Hz, 1H, H$_{2,ax}$), 3.52 (dd, J = 14.1, 2.7 Hz, 1H, H$_{4,eq}$), 3.26 (dd, J = 14.0, 4.8 Hz, 1H, H$_{4,ax}$), 2.98 (dd, J = 13.2, 1.6 Hz, 1H, H$_{2,eq}$), 1.68 (s, 3H, H$_5$), 1.35 (s, 3H, H$_1$); ^{13}C NMR (101 MHz, δ in acetone-*d6*): 171.3 (C$_7$), 158.7, 158.6, 157.6, 157.5 (all C$_q$), 154.9 (C$_{D6}$), 154.8 (C$_{A6}$), 152.3 (C$_{C6}$), 152.0 (C$_{B6}$), 140.0, 140.0, 140.0, 139.9 (C$_{A4}$+C$_{B4}$+C$_{C4}$+C$_{D4}$), 129.9, 129.2 (C$_{A5}$+C$_{D5}$), 128.9, 128.8 (C$_{B5}$+C$_{C5}$), 126.0, 125.8 (C$_{A3}$+C$_{D3}$), 125.3, 125.2 (C$_{B3}$+C$_{C3}$), 75.0 (C$_3$), 66.7 (C$_6$), 37.7 (C$_2$), 36.9 (C$_4$), 18.4 (C$_5$), 15.9 (C$_1$); HR-MS in CH$_3$CN m/z exp. (calc.): 312.0410 (312.0396, [M−2PF$_6$]$^{2+}$); UV-Vis: λ_{max} (ε in M^{-1}·cm^{-1}) in H$_2$O: 412 nm (5.18×10^3); Elemental analysis for C$_{27}$H$_{30}$F$_{12}$N$_4$O$_3$P$_2$RuS$_2$·3H$_2$O: (calc.): C, 33.51; H, 3.75; N, 5.79; (exp.): C, 34.91; H, 3.87; N, 5.89.

5.4.4 Density functional theory

Electronic structure calculations were performed using density functional theory (DFT) as implemented in the ADF software package (SCM). The structures of the sixteen possible Λ stereoisomers of [**1**](PF$_6$)$_2$, consisting of eight isomers with a chair-like metallacycle (i.e. *R* and *S* conformation for both sulfur atoms and the –OH substituent) and eight isomers with a boat-like metallacycle, were optimized in water using the conductor-like screening model (COSMO) to simulate the effect of solvation. The BLYP functional, combined with a TZP basis set, was employed in all calculations. All boat-like structures were found to convert to chair-like structures during the structure optimization process.

5.4.5 Photosubstitution quantum yields of [1–3](PF$_6$)$_2$ under blue-light irradiation

UV-Vis experiments on the ruthenium complexes were performed on a Cary 50 Varian spectrometer equipped with a Cary Single Cell Peltier for temperature control (T = 298 K) and stirring. For the irradiation, a LED light source was used (λ = 443 nm, FWHM = 11 nm) of which the photon flux was determined by ferrioxalate actinometry (see Table 5.4). Experiments were performed in 1.0 × 1.0 cm fluorescence cuvettes (QS-111, Hellma Analytics) containing 3.00 mL of solution. A stock solution of the desired complex was prepared using demineralized water, which was then diluted to the desired working concentration (Table 5.4) and placed in the cuvette. Irradiations were carried out under N$_2$ atmosphere after deoxygenation for 10 minutes by gentle bubbling of N$_2$ through the sample, and the sample was kept under inert atmosphere during the experiment by a gentle flow of N$_2$ over the top of the cuvette. A UV-Vis absorption spectrum was measured every 6 s during the experiment. Data was analysed using Microsoft Excel 2010. The quantum yields of the photosubstitution reactions (Φ_{443}) were calculated by fitting the time evolution of the UV-Vis absorption spectra of the irradiated solution using the Glotaran software package (see Appendix I).[10] Mass spectrometry (see section 3.4.1) was performed after the irradiation experiments to identify the photoproducts.

Table 5.4. Conditions of the photoreactions monitored by UV-Vis absorption spectroscopy and MS.

Entry	Complex	Solvent	[Ru] / μM	λ_{exc} / nm	q_p / mol·s^{-1}	t / min
1	[**1**](PF$_6$)$_2$	H_2O	72	443	2.65×10^{-8}	120
2	[**2**](PF$_6$)$_2$	H_2O	181	443	2.85×10^{-8}	120
3	[**3**](PF$_6$)$_2$	H_2O	99	443	2.85×10^{-8}	120

5.4.6 Singlet oxygen generation and phosphorescence quantum yield of [1](PF$_6$)$_2$

The singlet oxygen generation and phosphorescence quantum yields of [**1–4**](PF$_6$)$_2$ were determined as described in section 3.4.9.

5.5 References

[1] a) S. Bonnet, *Dalton Trans.* **2018**, *47*, 10330-10343; b) W. A. Velema, W. Szymanski, B. L. Feringa, *J. Am. Chem. Soc.* **2014**, *136*, 2178-2191; c) N. J. Farrer, L. Salassa, P. J. Sadler, *Dalton Trans.* **2009**, *38*, 10690-10701; d) S. Gai, G. Yang, P. Yang, F. He, J. Lin, D. Jin, B. Xing, *Nano Today* **2018**, *19*, 146-187; e) C. Mari, V. Pierroz, S. Ferrari, G. Gasser, *Chem. Sci.* **2015**, *6*, 2660-2686.

[2] a) F. Heinemann, J. Karges, G. Gasser, *Acc. Chem. Res.* **2017**, *50*, 2727-2736; b) J. Hess, H. Huang, A. Kaiser, V. Pierroz, O. Blacque, H. Chao, G. Gasser, *Chem. Eur. J.* **2017**, *23*, 9888-9896; c) G. Shi, S. Monro, R. Hennigar, J. Colpitts, J. Fong, K. Kasimova, H. Yin, R. DeCoste, C. Spencer, L. Chamberlain, A. Mandel, L. Lilge, S. A. McFarland, *Coord. Chem. Rev.* **2015**, *282-283*, 127-138; d) S. M. Cloonan, R. Elmes, M. Erby, S. A. Bright, F. E. Poynton, D. E. Nolan, S. J. Quinn, T. Gunnlaugsson, D. C. Williams, *J. Med. Chem.* **2015**, *58*, 4494-4505.

[3] a) L. Zayat, C. Calero, P. Alborés, L. Baraldo, R. Etchenique, *J. Am. Chem. Soc.* **2003**, *125*, 882-883; b) M. Frasconi, Z. Liu, J. Lei, Y. Wu, E. Strekalova, D. Malin, M. W. Ambrogio, X. Chen, Y. Y. Botros, V. L. Cryns, J.-P. Sauvage, J. F. Stoddart, *J. Am. Chem. Soc.* **2013**, *135*, 11603-11613; c) N. Karaoun, A. K. Renfrew, *Chem. Commun.* **2015**, *51*, 14038-14041; d) J.-A. Cuello-Garibo, M. S. Meijer, S. Bonnet, *Chem. Commun.* **2017**, *53*, 6768-6771; e) F. Battistin, G. Balducci, J. Wei, A. K. Renfrew, E. Alessio, *Eur. J. Inorg. Chem.* **2018**, *2018*, 1469-1480; f) L. Kohler, L. Nease, P. Vo, J. Garofolo, D. K. Heidary, R. P. Thummel, E. C. Glazer, *Inorg. Chem.* **2017**, *56*, 12214-12223; g) L. M. Loftus, K. F. Al-Afyouni, C. Turro, *Chem. Eur. J.* **2018**, *24*, 11550-11553; h) A. Li, R. Yadav, J. K. White, M. K. Herroon, B. P. Callahan, I. Podgorski, C. Turro, E. E. Scott, J. J. Kodanko, *Chem. Commun.* **2017**, *53*, 3673-3676; i) G. Ragazzon, I. Bratsos, E. Alessio, L. Salassa, A. Habtemariam, R. J. McQuitty, G. J. Clarkson, P. J. Sadler, *Inorg. Chim. Acta* **2012**, *393*, 230-238.

[4] J. K. White, R. H. Schmehl, C. Turro, *Inorg. Chim. Acta* **2017**, *454*, 7-20.

[5] a) R. E. Goldbach, I. Rodriguez-Garcia, J. H. van Lenthe, M. A. Siegler, S. Bonnet, *Chem. Eur. J.* **2011**, *17*, 9924-9929; b) A. Bahreman, M. Rabe, A. Kros, G. Bruylants, S. Bonnet, *Chem. Eur. J.* **2014**, *20*, 7429-7438; c) B. Siewert, M. Langerman, A. Pannwitz, S. Bonnet, *Eur. J. Inorg. Chem.* **2018**, *2018*, 4117-4124.

[6] a) S. Bonnet, J. P. Collin, N. Gruber, J. P. Sauvage, E. R. Schofield, *Dalton Trans.* **2003**, *0*, 4654-4662; b) L. Zayat, O. Filevich, L. M. Baraldo, R. Etchenique, *Phil. Trans. R. Soc. A* **2013**, *371*, 20120330.

[7] a) J.-A. Cuello-Garibo, C. C. James, M. A. Siegler, S. Bonnet, *Chem. Sq.* **2017**, *1*, 2; b) R. N. Garner, L. E. Joyce, C. Turro, *Inorg. Chem.* **2011**, *50*, 4384-4391; c) J.-P. Collin, D. Jouvenot, M. Koizumi, J.-P. Sauvage, *Inorg. Chim. Acta* **2007**, *360*, 923-930; d) N. A. F. Al-Rawashdeh, S. Chatterjee, J. A. Krause, W. B. Connick, *Inorg. Chem.* **2014**, *53*, 294-307; e) M. J. Root, B. P. Sullivan, T. J. Meyer, E. Deutsch, *Inorg. Chem.* **1985**, *24*, 2731-2739; f) S. H. C. Askes, M. S. Meijer, T. Bouwens, I. Landman, S. Bonnet, *Molecules* **2016**, *21*, 1460.

[8] M. E. Fleet, *Mineral. Mag.* **1976**, *40*, 531-533.

[9] a) R. N. Garner, J. C. Gallucci, K. R. Dunbar, C. Turro, *Inorg. Chem.* **2011**, *50*, 9213-9215; b) A. Zamora, C. A. Denning, D. K. Heidary, E. Wachter, L. A. Nease, J. Ruiz, E. C. Glazer, *Dalton Trans.* **2017**, *46*, 2165-2173; c) D. V. Pinnick, B. Durham, *Inorg. Chem.* **1984**, *23*, 1440-1445.

[10] J. J. Snellenburg, S. Laptenok, R. Seger, K. M. Mullen, I. H. M. van Stokkum, *J. Stat. Softw.* **2012**, *49*, 22.

[11] E. J. Corey, B. W. Erickson, R. Noyori, *J. Am. Chem. Soc.* **1971**, *93*, 1724-1729.